All-Optical Multi-Channel Aggregator for QPSK to 16QAM Based on Time-Lens and Phase Reloader in Elastic Optical Networks

Yu Ding, Hongxiang Wang, Yuefeng Ji, and Yu Zhang

***Abstract*—An all-optical aggregator consisting of time-lens and a phase reloader for two four-channel multiplexed quadrature phase shift keying (QPSK) signals to a wavelength division multiplexed (WDM) 16-ary quadrature amplitude modulation (16QAM) signal is proposed. The feasibility of the scheme is confirmed by the waveforms of the intermediate process and the constellations of input-output signals. The performance of bit error rate (BER) and error vector magnitude (EVM) values under different optical signal-to-noise ratios (OSNR) are analyzed to evaluate the system, and the OSNR penalties of the aggregated signal at the forward error correction (FEC) threshold are between 2.25 dB and 2.45 dB. This scheme potentially enables reconfigurable service and improves compatibility in elastic optical networks (EON).**

***Index Terms*—All-optical, multi-channel aggregator, OFT.**

I. Introduction

In RECENT years, services such as Big Data, cloud computing, and artificial intelligence have ushered in a period of rapid development. According to forecasts, global Internet users will likely reach 5 billion [1]. Diverse services types and increasing user access devices jointly pose new challenges to the carrying capacity of optical networks. Therefore, elastic optical networks (EON) with advantages such as large transmission capacity, flexible resource allocation and high spectral efficiency have become the future trend [2]. Furture elastic optical networks that are heterogeneous and re-configurable will have variable bandwidth and can dynamically adjust the modulation format according to different network characteristics and quality of service (QoS), which requires the network nodes to have flexible signal processing functions. However, traditional network nodes process signals in the electrical domain, involving multiple inefficient photoelectric conversion processes. All-optical signal processing technology can break through the limitations of electronics [3], so the application of all-optical nodes will be of great significance in EON.

The diversity of services requires the diversity of modulation formats, resulting in the coexistence of multiple modulation formats in EON. Advanced modulation formats with higher spectral efficiency can carry high-traffic services in core and metro networks [4]. In contrast, low-order modulation formats with more robust anti-noise performance are more appropriate in short-haul access networks [5]. Aggregation and de-aggregation techniques can synthesize lower-order channels and decompose higher-order channels at the gateways of different networks to achieve recofigurable and efficient service grooming, enhancing the compatibility between different types of networks. All-optical aggregation and de-aggregation can avoid frequent photoelectric conversions and significantly improve processing efficiency. Several all-optical aggregation schemes between identical or different formats have been proposed. For example, the conversion from multiple on-off keying (OOK) signals to a quadrature phase shift keying (QPSK), an 8-ary phase shift keying (8PSK) [6], or a 16-ary quadrature amplitude modulation (16QAM) [7] by cross-phase modulation (XPM); four binary phase shift keying (BPSK) signals to a 16QAM using the coherent addition of optical vector signals [8]; multiple QPSKs to a 16QAM [9] or a 64-ary quadrature amplitude modulation (64QAM) [10] by sum frequency generation (SFG) and difference frequency generation (DFG) effects in periodically poled lithium niobate (PPLN). On the other hand, an OOK and a differential QPSK (DQPSK) to an 8-ary amplitude and phase shift keying (8-APSK) by four-wave mixing (FWM) in highly nonlinear fiber (HNLF) [11], an OOK and a QPSK to an 8-ary quadrature amplitude modulation (8QAM) by XPM and cross-gain modulation (XGM) in semiconductor optical amplifier (SOA) [12], an OOK and a BPSK to a QPSK by XPM [13], [14], and an amplitude shift keying (ASK) and a BPSK to an 8QAM by FWM in HNLF [15]. However, these schemes only focus on the single channel and cannot be directly applied to the multi-channel signals.

Wavelength division multiplexed (WDM) technology provides huge transmission capacity for optical networks and wavelength is the smallest granularity for transmission and switching. However, WDM signals suffer from inter-channel crosstalk and

Manuscript received 4 October 2022; revised 7 November 2022; accepted 8 November 2022. Date of publication 14 November 2022; date of current version 21 November 2022. This work was supported in part by the National Key Research and Development Program of China under Grant 2019YFB1803601, in part by the National Natural Science Foundation of China under Grant 62021005, and in part by the Beijing Natural Science Foundation under Grant Z210004. *(Corresponding author: Hongxiang Wang.)*

Yu Ding, Hongxiang Wang, and Yuefeng Ji are with the State Key Laboratory of Information Photonics and Optical Communications, School of Information and Communication Engineering, Beijing University of Posts and Telecommunications, Beijing 100876, China (e-mail: dingyu@bupt.edu.cn; wanghx@bupt.edu.cn; jyf@bupt.edu.cn).

Yu Zhang is with the Academy of Broadcasting Science, NRTA, Beijing 102206, China (e-mail: sakas.zhang@hotmail.com).

Digital Object Identifier 10.1109/JPHOT.2022.3221796

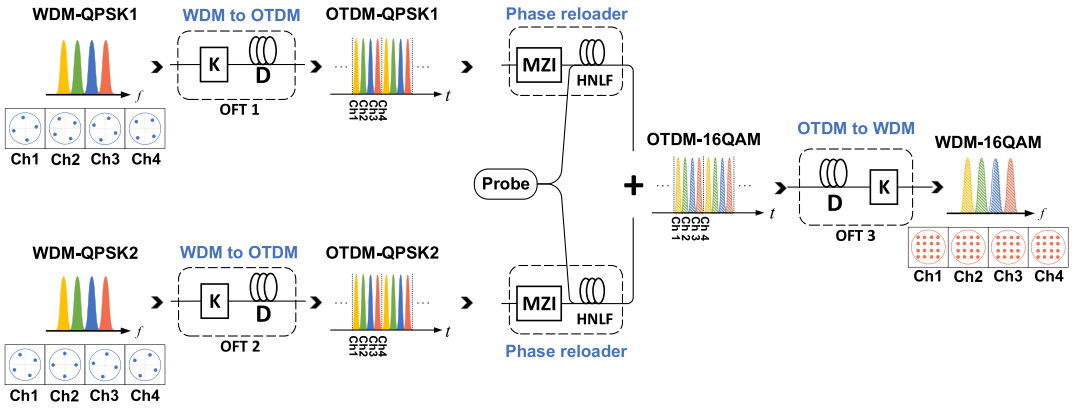

Fig. 1. Scheme of all-optical WDM signal aggregator. The two input signals with random inter-channel carrier phases are transformed into OTDM signals by the first OFT and phase reloader, and then after aggregation and the second OFT, a phase-synchronized output signal between channels can be obtained.

complex nonlinear interference during transmission. Therefore, several schemes have been proposed to suppress excess nonlinear crosstalk. For example, the polarization-assisted scheme needs to isolate WDM channels with different polarization and propagation directions [16], which is not suitable for WDM signals with equal frequency spacing and cannot be scaled to more wavelength channels. In [17], a group delay managed (GDM) nonlinear medium with inter-channel discontinuous dispersion and intra-channel near-zero dispersion can suppress XPM and FWM effects, but it is only sensitive to intensity-modulated signal. In [18], the WDM signals are transformed to the OTDM signals using the optical Fourier transformer (OFT), but subsequent operations make the whole processing technique valid only for BPSK. For the aggregated multi-channel signals, the corresponding processing scheme should not only suppress crosstalk, but also maintain phase synchronization between different channels.

In this paper, we propose a multi-channel aggregator for QPSKs to 16QAM consisting of time-lens and a phase reloader. Here, the time-lens can achieve conversion between WDM and optical time division multiplexed (OTDM), which effectively alleviates inter-channel interference during processing while ensuring the integrity of the information. The phase reloader can modulate the information onto the local probe to achieve inter-channel phase synchronization. The proposed system aggregates two four-channel multiplexed QPSK signals at 25 Gbaud per channel to four standard square 16QAM signals. The time and frequency domain waveforms, and the input-output constellations demonstrate the feasibility of the scheme. Finally, the bit error rate (BER) and error vector magnitude (EVM) under different optical signal-to-noise ratios (OSNR) are analyzed to evaluate the system performance.

II. Operation Principle

The aggregation scheme for WDM-QPSK1 and WDM-QPSK2 to WDM-16QAM is shown in Fig. 1. Taking one of the WDM signals as an example, it is first transformed into a single wavelength OTDM signal by OFT, thereby shielding most of the interference of nonlinear effects. Then the phase information of the QPSK signal are transformed into four intensities by a Mach-Zehnder Interferometer (MZI), and the probe is modulated into a new QPSK signal by XPM in HNLF. The same operation is done for the other WDM signal. The 16QAM is generated by aggregating two QPSK signals with a power ratio of 1:4. So the two OTDM-QPSK signals are coupled to generate the OTDM-16QAM signal. Finally, it is transformed to WDM-16QAM by OFT and the different channels are phase-synchronized.

A. OFT Based on Time-Lens

Space-time duality reveals the correspondence of optical phenomena in these two dimensions. The diffraction of light waves in the space dimension can be analogous to the propagation of signals in the dispersive medium in the time dimension, while the space lens corresponds to the time-lens [19]. Like the space lens function, the time-lens is essentially a structure for the quadratic phase modulation of the optical signal. The time domain transfer functions of the dispersive effect and the time-lens are:

$$h_D(t) = \sqrt{j\frac{1}{2\pi D}} \cdot e^{-j\frac{t^2}{2D}} \tag{1}$$

$$h_K(t) = e^{-j\frac{Kt^2}{2}} \tag{2}$$

where D is group delay dispersion (GDD) and K is chirp.

In this scheme, the first OFT only needs to realize the transformation of the input frequency domain to the output time domain. As shown in Fig. 2, the incomplete Fourier transform system is composed of "chirp + dispersive medium" [20]. The input signal passes through a quadratic phase-modulation with chirp factor K, and then through a dispersive medium with group velocity dispersion (GVD) β and length L. The complex electric field amplitude relationship between the output and input signals can be expressed as

$$\begin{aligned} A(L,t) &= A(0,t)h_K(t) * h_D(t) \\ &= \sqrt{\frac{j}{2\pi D}} e^{-\frac{jt^2}{2D}} \int_{-\infty}^{+\infty} A(0,\tau) e^{-\frac{jK\tau^2}{2}} e^{-\frac{j\tau^2}{2D}} e^{\frac{jt\tau}{D}} d\tau \end{aligned} \tag{3}$$

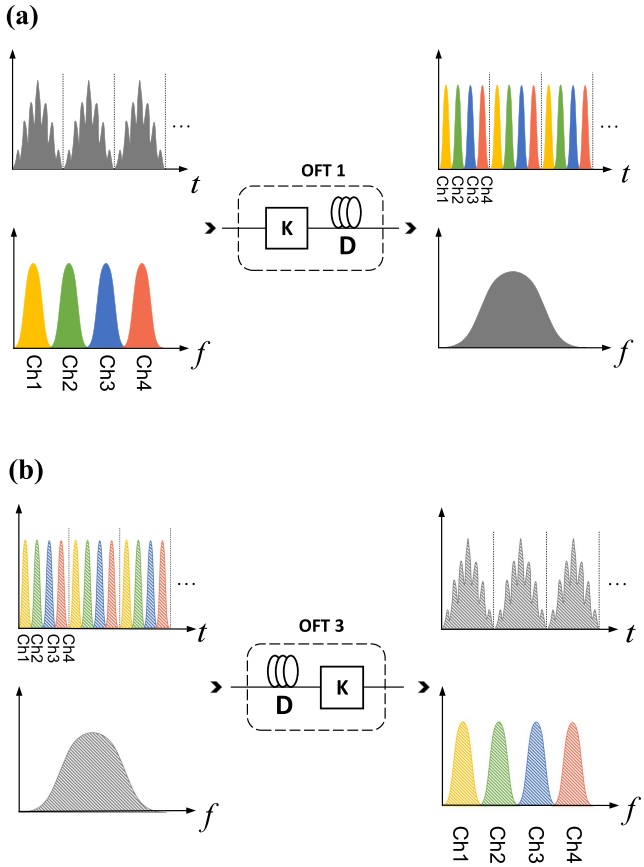

Fig. 2. Comparison of input and output signals in the time and frequency domains. (a) Input and output temporal waveform and spectrograms of the first OFT process; (b) Input and output temporal waveform and spectrograms of the last OFT process.

When $K = -1/D$, the two terms $e^{-jK\tau^2/2}$ and $e^{-j\tau^2/2D}$ in (3) can cancel each other, and the output signal can be calculated as:

$$A(L,t) = \sqrt{\frac{j}{2\pi D}} e^{-\frac{jt^2}{2D}} \cdot \tilde{A}(0,\omega)\omega_{\omega=\frac{t}{D}} \tag{4}$$

where $\tilde{A}(0,\omega)$ refers to the frequency domain expression of the input signal. Equation (4) shows that the time domain waveform of the output signal is the same as the frequency domain waveform of the input signal.

As shown in Fig. 2(b), the second OFT in the scheme is an incomplete Fourier transform system composed of "dispersive medium + chirp," which can only transform the input frequency domain to the output time domain waveform [20]. According to (1) and (2), the frequency domain transfer functions of the dispersion effect and the quadratic phase-modulation are $H_D(\omega) = e^{j\omega^2 D/2}$ and $H_K(\omega) = \sqrt{j \cdot 2\pi/K} \cdot e^{j\omega^2/2K}$, respectively, and the output signal can be expressed as:

$$\begin{aligned}\tilde{A}(L,\omega) &= \frac{1}{2\pi}\tilde{A}(0,\omega)H_D(\omega) * H_K(\omega) \\ &= \sqrt{\frac{j}{2\pi K}} e^{\frac{j\omega^2}{2K}} \int_{-\infty}^{+\infty} \tilde{A}(0,\omega') e^{\frac{jD\omega'^2}{2}} e^{\frac{j\omega'^2}{2K}} e^{-\frac{j\omega\omega'}{K}} d\omega'\end{aligned} \tag{5}$$

where $\tilde{A}(L,\omega)$ refers to the frequency domain expression of the output signal. When $D = -1/K$, the two terms $e^{jD\omega'^2/2}$ and $e^{j\omega'^2/2K}$ in (5) can cancel each other, and the output signal can be calculated as:

$$\tilde{A}(L,\omega) = \sqrt{\frac{j \cdot 2\pi}{K}} e^{\frac{j\omega^2}{2K}} \cdot A(0,t)_{t=\frac{\omega}{K}} \tag{6}$$

This indicates that the frequency domain waveform of the output signal is the same as the time domain waveform of the input signal.

The FWM effect is used to realize the time-lens with a quadratic phase transfer function. The signal at ω_s and the pump at ω_p will generate an idler at $\omega_i = 2\omega_p - \omega_s$, and the relationship between the three electric fields is:

$$E_i = \eta E_s^* E_p^2 \tag{7}$$

where η is the FWM efficiency. Equation (7) shows that idler carries the conjugate phase of the signal and the double phase of the pump, i.e., $\varphi_i = 2\varphi_p - \varphi_s$. The pump with quadratic phase function can be obtained by dispersion. When the chirp-free Gaussian pulses pass through the dispersive medium with $D_p = \beta_2 L_p$, if the condition for far-field Fraunhofer diffraction is satisfied [21], the phase function of the pump is:

$$\varphi_p(t) = -\frac{t^2}{2D_p} \tag{8}$$

The aperture of such time-lens can be expressed as:

$$\Delta T = \frac{|D_p|}{\sqrt{2}} \cdot 2\pi\Delta f \tag{9}$$

The aperture should be larger than the duration of the signal to achieve distortion-free conversion. Since the idler has twice the pump phase added, the transfer function of the lens is:

$$h_K(t) = e^{2j\varphi_p(t)} = e^{-j\frac{t^2}{D_p}} \tag{10}$$

By comparing (2) and (10), the chirp factor of the FWM-based time-lens can be calculated as $K = 2/D_p$.

B. Phase Reloader

The main idea of the phase reloader is derived from the phase regenerator without active phase locking [22] and all-optical conversion from PAM4 to 16QAM [26], which consists of two conversion processes, as shown in Fig. 3. First, the phase signal is transformed into an intensity-modulated signal by an MZI with time delay of one symbol and phase shift of φ_d in the upper and lower arms, respectively. The electric field relationship between the output and the input signal is:

$$\begin{aligned}E_{\text{out}} &= E_{\text{in}} \cdot e^{j\omega T} + j \cdot j \cdot E_{\text{in}} e^{j\varphi_d} \\ &= E_{\text{in}} \cdot e^{j\frac{\omega T + \varphi_d}{2}} \cdot \sin\left(\frac{\omega T - \varphi_d}{2}\right)\end{aligned} \tag{11}$$

Equation (11) shows that the intensity of output signal is only related to the input signal intensity and the independent variable in sine function. If φ_d is equal to zero, the value $\omega T - \varphi_d = 0, \pm\pi/2, \pi$ and the output signal has only three intensity values. Therefore, we make the MZI output four intensities by adjusting

TABLE I
MAIN PARAMETERS IN THE SYSTEM

	SMF1	DCF1	HNLF1	SMF2	SMF3
Nonlinear coefficient γ $(W^{-1}km^{-1})$	1.3	1.3	13	1.3	1.3
Dipersion parameter β_2 (ps^2/km)	-20	20	-0.4	-20	-20
dispersion slop S $(ps/nm^2/km)$	0.05	-0.05	0.02	0.05	0.05
Length L (m)	390	780	100	390	780

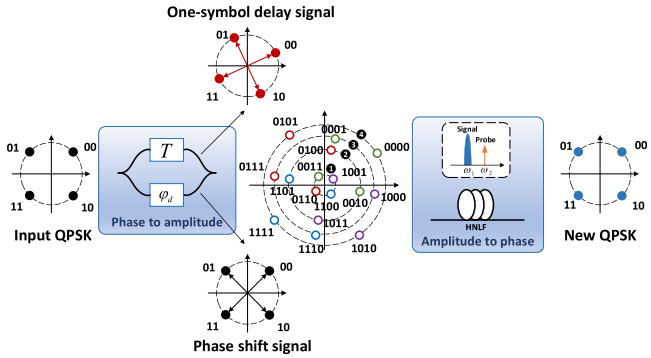

Fig. 3. Scheme of phase reloader with constellation diagrams. The input QPSK signal is transformed into a four-amplitude signal after MZI, and then the probe is modulated into a new QPSK in HNLF.

the value of φ_d. The four-intensity signal can be used as a pump to modulate the local probe into a four-phase signal according to the property that phase shift during XPM effect depends on intensity. However, during the pump-probe interaction, we cannot consider the XPM effect in isolation, and other nonlinear effects can perturb the results, so the actual power and phase of the output signal are [23]:

$$P_{\text{out}} = P_0 J_1^2\left(2\sqrt{P_0 P_1}\gamma L_n\right) + P_1 J_0^2\left(2\sqrt{P_0 P_1}\gamma L_n\right) \quad (12)$$

$$\varphi_{\text{out}} = \varphi_1 + \gamma L_n P_0 + \gamma L_n P_1 + \arctan\left\{\frac{\sqrt{P_0}J_1\left(2\sqrt{P_0 P_1}\gamma L_n\right)}{\sqrt{P_1}J_0\left(2\sqrt{P_0 P_1}\gamma L_n\right)}\right\} \quad (13)$$

where P_0 and P_1 are the power of the pump and probe, γ and L_n are the nonlinear coefficient and length of the medium, $J_n(x)(n = 0, 1)$ refers to the nth-order Bessel function, and φ_1 is the initial phase of the probe. The two terms $\gamma L P_0$ and $\gamma L P_1$ in (13) refer to XPM and SPM, and the last term refers to Bessel-order mixing (BOM). The perturbation caused by the SPM and FWM effects can be reduced by choosing the appropriate L_n, P_0 and P_1.

III. SETUP AND RESULTS

Fig. 4(a) shows the simulation configuration of the all-optical aggregation for two WDM-QPSKs to WDM-16QAM. The main parameters used in the simulation are shown in Table I. At the transmitter of the WDM to OTDM converter, four continuous wave (CW) lasers in the frequency range from 192.3 THz to 192.9 THz with a frequency interval of 200 GHz are modulated with IQ modulators. Four QPSK signals are multiplexed as WDM-QPSK1 with a single channel symbol rate of 25 Gbaud. WDM-QPSK2 has the same number of channels and symbol rate as WDM-QPSK1, with a frequency range from 194.7 THz to 195.3 THz. To be specific, controllable amount of amplifier spontaneous emission (ASE) noise is added to the input QPSK signals to evaluate the performance of the system by coupling ASE noise source with the input signals. To avoid the aperture limitation of electro-optic modulation schemes, a time-lens scheme based on single-pump FWM is adopted. The pulsed laser at 193.8 THz emits an initial pulse sequence with a 25 GHz repetition rate. Then the pulse sequence is shaped by the pulse shaper into a Gaussian shape with a full width at half maximum (FWHM) of 4 ps and zero phase and instantaneous frequency, as shown in Fig. 4(b). The Gaussian pulses are filtered by a band-pass filter (BPF) and then transmitted through a dispersion compensating fibers (DCF) with $\beta_2 = 20\ \text{ps}^2/\text{km}$ and $L = 780$ m as the pump for the FWM-based time-lens whose aperture satisfies the requirement of distortion-free conversion. Fig. 4(c) illustrates that each sequence pulse corresponds to a parabolic phase curve and an approximately linear instantaneous frequency curve. The sequence is divided into two paths used as pumps for WDM-QPSK1 and WDM-QPSK2. Time synchronization between WDM-QPSK and pump is adjusted with the optical tunable delay line (TDL), while the polarization controller (PC) is used to make both have the same polarization. The signals and pump are injected into HNLF with $\gamma = 13$ $\text{W}^{-1}\text{km}^{-1}$, the generated idlers are filtered out by BPF. Then the two idlers are converted into OTDM-QPSK1 and OTDM-QPSK2 by passing through the single-mode fiber (SMF) with $\beta_2 = -20\ \text{ps}^2/\text{km}$ and $L = 390$ m. For achieving the OFT, the relation of $K = -1/D$ is necessary. The length of DCF fiber is twice as long as SMF and the group velocity dispersion satisfies the condition of the inverse sign. Fig. 5(a) shows the time and frequency domain diagrams of the WDM to OTDM converter. As shown in Fig. 5(b), the four-channel WDM-QPSK1 interacte with the pump in the HNLF and the generated idler located at 195.0 THz. Fig. 5(c) shows the OTDM-QPSK waveforms after the SMF, one symbol period (40 ps) of the original input signal is divided into four time slots, and each carries information of one channel. The spectra of the interaction between WDM-QPSK2 and the pump is similar to that in Fig. 5(d).

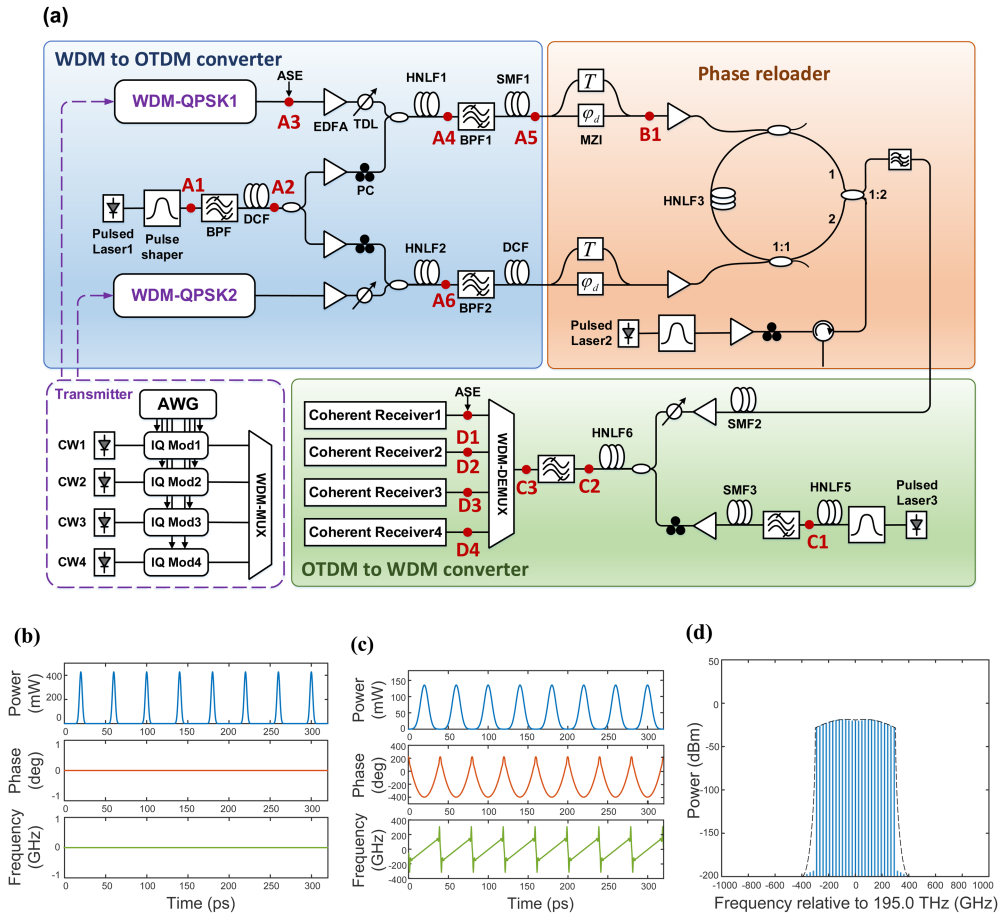

Fig. 4. (a) Simulation configuration of all-optical WDM signal aggregator; (b) and (c) are the corresponding waveforms, phases, and instantaneous frequencies at A1 and A2 respectively; (d) spectra of broadband flat-top pump pulses at C1.

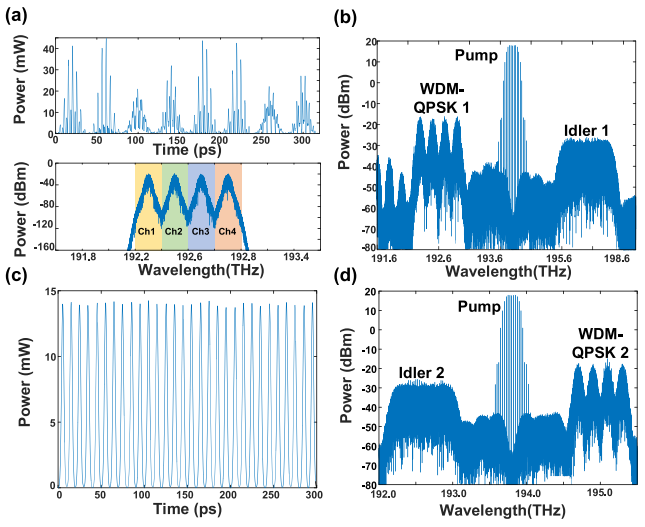

Fig. 5. Waveform diagrams of the corresponding points in the WDM to OTDM converter. (a) time and frequency domain waveforms of the input WDM-QPSK1 at A3; (b) spectra of WDM-QPSK1, pump, and idler of the FWM process after HNLF at A4; (c) time domain waveforms of the converted OTDM-QPSK1 at A5; (d) spectra of WDM-QPSK2, pump, and idler of FWM the process after HNLF at A6.

At the phase reloader, the two OTDM-QPSK signals are transformed into four-amplitude signals by MZI with $T = 40$ ps and $\varphi_d = \pi/9$, and the average power of the signals is amplified to 0.53 W by erbium doped fiber amplifier (EDFA). The phase-locked between two four-amplitude signals is also a critical problem in the practical implementation, because the relative phase may be affected by the unequal optical paths before the coherent addition. The environmental impact on the relative phase between both arms is necessary to be taken into consideration, an active phase-locking loop and the nonlinear optical loop mirror (NOLM) scheme should be designed in the practical implementation [27], or the on-chip scheme is another effective approach to settle this issue. The phase reloader mainly consists of the NOLM and a 1:2 optical coupler. The Gaussian pulse sequence at 193.8 THz is injected in the NOLM from the coupler and amplified to 0.02 W as probes. The probe pulse sequence is set to 1 ps full width at half maximum at 100 GHz repetition rate according to the rate of the OTDM signals. After injected in the NOLM, the probe pulses which are split into port 1 and 2 respectively, will travel through the loop, clockwise and counter-clockwise. The clockwise four-amplitude signal 1 is used to modulate the probe pulse into QPSK1 by XPM in HNLF. In the same way, the probe pulse propagating couter-clockwise

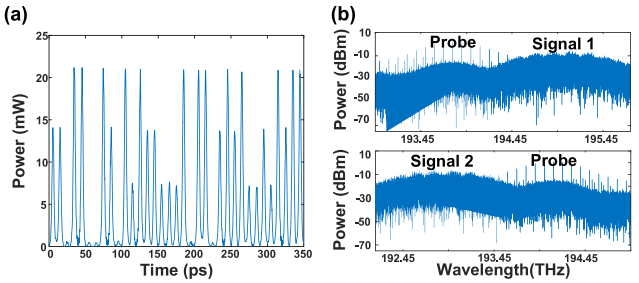

Fig. 6. Waveform diagrams of the corresponding points in the phase reloader. (a) time domain waveform of four-amplitude OTDM signal after MZI at B1; (b) are spectra of signal-probe of XPM process after HNLF.

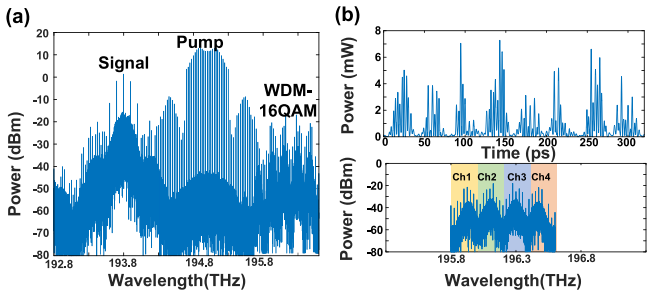

Fig. 7. Waveform diagrams of the corresponding points in the OTDM to WDM converter. (a) the spectra of signal, pump, and idler of the FWM process after HNLF at C2; (b) time and frequency domain waveforms of the converted WDM-16QAM at C3.

is coupled with the four-amplitude signal 2 and converted to QPSK2. Each signal-probe is time-synchronized and polarized identically by TDL and PC, interacting in the HNLF with a length of 100 m. Subsequently, the converted QPSK signals 1 and 2 are coupled by 1:2 optical coupler and the converted 16QAM signal can be obtained by extracting the probe pulse using an BPF. The temporal waveform of the signals after MZI is shown in Fig. 6. As shown in Fig. 6(a), the signal has four intensities, which confirms the theory mentioned above in Section II. The spectra of the XPM effect clockwise and counter-clockwise are shown in Fig. 6(b).

At the OTDM to WDM converter, the OTDM-16QAM passes through a SMF with $\beta_2 = -20$ ps^2/km and $L = 390$ m. Since the spectral envelope of the converted WDM signal will be related to the pump shape, the Gaussian pulses with FWHM of 4 ps at 195.0 THz are spectrally broadened and filtered to obtain a broadband flat-top sequence [24], as shown in Fig. 4(d), then passes through the SMF with $\beta_2 = -20$ ps^2/km and $L = 780$ m as the pump pulses. The synchronized signal and pump are combined into the HNLF, and the generated WDM-16QAM is filtered out at 196.2 THz. After wavelength demultiplexing, four channels of WDM-16QAM can be coherently received at frequencies of 195.9 THz, 196.1 THz, 196.3 THz, and 196.5 THz, respectively. Coherent detection and offline DSP process are applied in our scheme to recover the constellation map and calculate the bit error rate. In the DSP process, we performed IQ orthogonalization, clock recovery, channel equalization based on constant modulus algorithm (CMA), phase recovery based on BPS (blind phase search) algorithm, and bit error rate calculation. Fig. 7(a) shows the spectra of the WDM-16QAM generated by the interaction of the signal and the pump. The time and frequency domain waveforms of th signal in Fig. 7(b) are consistent with the expected output results in Fig. 2(b). In the simulation, we can do the corresponding differential processing on the input PRBS offline at Rx when we use a PRBS. However, the QPSK should be precoded as a DQPSK in the practical system because the bit sequence changes through a MZI.

The constellations of the two input four-channel WDM-QPSK signals with input noise and the aggregated WDM-16QAM under the OSNR of 23 dB are shown in Fig. 8. After the MZI, the intensity and phase noise of the original QPSK signals are converted to the intensity noise. Then the intensity noise will be converted to the phase noise due to XPM during the phase reloading. In addition, it is worth noting that the delay jitter of the MZI will affect the intensity distribution of the converted intensity-modulated signal in the experiments. The average phase deviations of the input signals from the same reference constellation range from 0 to 75 degrees, and the EVMs range from 4.3% to 4.5%. Eight QPSK signals with phase error of 5.66 ° and amplitude error of 2.11% can be aggregated into four standard square 16QAM signals after system processing. The average phase deviations of the four synchronized 16QAM signals range from 0.46 to 0.82°, and the EVMs range from 11.9% to 12.4%. Furthermore, signal of channel 1 with different levels of noise (OSNR=22 dB and 18 dB) is coupled with ASE source and the aggregated 16QAMs are demonstrated to as shown in Fig. 9. Since the output signals accumulate the amplitude and phase noise of the two aggregated signals, the quality of the aggregated signals is degraded compared to the input signals. As the phase noise of the input QPSK signal increases, the converted amplitude fluctuations will also get bigger, especially for the high amplitude. Due to the XPM, the high amplitude will induce greater phase noise. The phase noise of the four central points on the constellation gradually increases in the clockwise direction.

As shown in Fig. 4(a), ASE noises are added to the point D1, D2, D3, and D4 to vary the received OSNR to evaluate the noise tolerance of the aggregated 16QAMs. The corresponding BER and EVM values versus receiver OSNR are calculated, and the curves are shown in Fig. 10. The figure includes back-to-back (B2B) reference curves [25] and received 16QAM curves per channel under the OSNR of 25 dB. When the forward error correction (FEC) threshold is $10^{-2.4}$, the OSNRs of the aggregated signals are degraded by about 2.25∼2.45 dB compared with the B2B signal. In Fig. 10(b), the EVMs of the received 16QAMs are between 16.9% and 17.5% when OSNR = 19 dB. The degradation of OSNRs and the EVMs indicates that the aggregated signal has been introduced noise during the phase reloader.

The scheme can achieve the aggregation of MPSK. The MPSK signal is converted into an intensity-modulated signal with multiple amplitudes and approximately uniform intervals

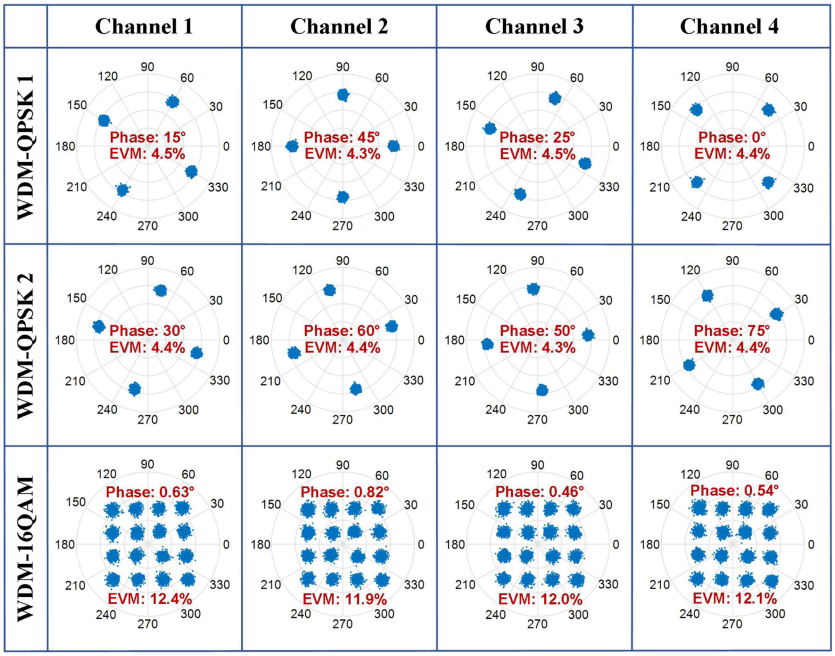

Fig. 8. Input and output constellations of the all-optical WDM signal aggregator. The multi-channel input signals with disordered carrier phases aggregate the square 16QAM signal with phase synchronization.

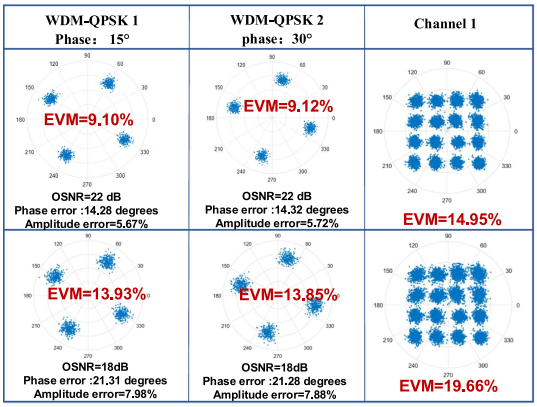

Fig. 9. Input and output constellations of Channel 1 under different levels of ASE noise.

by adjusting the phase shift of the MZI. After changing the output power of the signal and the probe, the synchronized MPSK signals can be reloaded.

In the simulation, we use the VPItransmissionmaker Optical system (VPI) to build the simulation system, which can provide mixed programming and advanced models to perform complex simulations for high-speed optical communication system. The system simulation is implemented by solving the coupled nonlinear Schroedinger (NLS) equation describing the lightwave propagation in fibers using the split-step Fourier method. We mainly consider the following nonlinear processes during the signal process: FWM, SPM, and XPM. Other nonlinear effects, such as stimulated Brillouin scattering (SBS) and stimulated Raman scattering (SRS) are not taken into consideration.

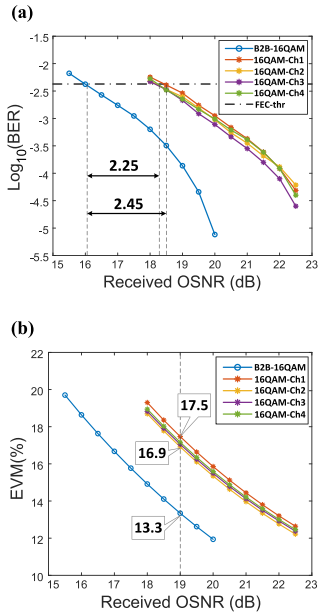

Fig. 10. (a) BER and (b) EVM curves of the all-optical WDM signal aggregator.

IV. Conclusion

This paper proposed an all-optical multi-channel aggregator consisting of time-lens and phase reloaders to combine two WDM-QPSKs to a WDM-16QAM. The principles of time-lens and phase reloader have been analyzed, and the aggregation of two four-channel multiplexed QPSK signals at 25 Gbaud per channel has been simulated. The system function has been

verified through the time and frequency domain waveforms and input-output constellation diagrams of the intermediate process. In addition, the phase deviation values of the aggregated signals are between 0.46° and 0.82°. The performance of the system is evaluated through the BER and EVM curves. According to the results, the OSNR of the aggregated 16QAM signals should be over ∼18.5 dB to meet the BER threshold under FEC limit. The proposed system realizes the multi-channel aggragation and has potential application in service convergence node to enable efficient service grooming.

REFERENCES

[1] T. Barnett, S. Jain, U. Andra, and T. Khurana, "Cisco visual networking index (VNI) complete forecast update, 2017–2022," in *Proc. Amer./EMEAR Cisco Knowl. Netw. Presentation*, 2018, pp. 1–30.

[2] O. Gerstel, M. Jinno, A. Lord, and S. J. B. Yoo, "Elastic optical networking: A new dawn for the optical layer?," *IEEE Commun. Mag.*, vol. 50, no. 2, pp. s12–s20, Feb. 2012.

[3] J. Yuefeng, W. Hongxiang, C. Y. J. Meitong, Y. Zhitian, and B. Lin, "All-optical signal processing technologies in flexible optical networks," *Photon. Netw. Commun.*, vol. 38, no. 1, pp. 14–36, 2019.

[4] P. J. Winzer, "High-spectral-efficiency optical modulation formats," *J. Lightw. Technol.*, vol. 30, no. 24, pp. 3824–3835, Dec. 2012.

[5] P. Limeng, W. Hongxiang, and J. Yuefeng, "All-optical deaggregation from 8PSK to 3× BPSK based on FWM in HNLF," *Appl. Opt.*, vol. 58, no. 5, pp. 1246–1252, 2019.

[6] K. Mishina, S. Kitagawa, and A. Maruta, "All-optical modulation format conversion from on-off-keying to multiple-level phase-shift-keying based on nonlinearity in optical fiber," *Opt. Exp.*, vol. 15, no. 13, pp. 8444–8453, 2007.

[7] K. Mishina, S. Kitagawa, A. Maruta, and K. Kitayama, "All-optical OOK-to-16QAM format conversion by using SOA-MZI wavelength converters," in *Proc. 17th Opto- Electron. Commun. Conf.*, 2012, pp. 337–338.

[8] W. Hongxiang, P. Limeng, and J. Yuefeng, "All-optical aggregation and de-aggregation of 4× BPSK-16QAM using nonlinear wave mixing for flexible optical network," *IEEE J. Sel. Topics Quantum Electron.*, vol. 27, no. 2, pp. 1–8,Mar./Apr. 2021.

[9] A. Mohajerin-Ariaei et al., "Demonstration of multiplexing and transmission of QPSK-to-16QAM channels over 100 km using wave mixing for aggregation and noise mitigation," *IEEE J. Sel. Topics Quantum Electron.*, vol. 27, no. 2, pp. 1–8, 2019.

[10] A. Fallahpour et al., "Experimental generation of a 64-QAM by optically aggregating three independent QPSK channels using nonlinear wave mixing of multiple Kerr comb lines," in *Proc. CLEO: Appl. Technol.*, 2017, pp. JTh2A–59.

[11] G. W. Lu and T. Miyazaki, "Experimental demonstration of RZ-8-APSK generation through optical amplitude and phase multiplexing," *IEEE Photon. Technol. Lett.*, vol. 20, no. 23, pp. 1995–1997, Dec. 2008.

[12] K. Hiroki, U. Masaki, and G. Nobuo, "All-optical modulation format conversion between OOK, QPSK, and 8QAM," *J. Lightw. Technol.*, vol. 37, no. 16, pp. 3925–3931, Aug. 2019.

[13] L. Hong, W. Hongxiang, X. Zhen, and J. Yuefeng, "Simultaneous all-optical channel aggregation and de-aggregation based on nonlinear effects for OOK and MPSK formats in elastic optical networking," *Opt. Exp.*, vol. 27, no. 20, pp. 30158–30171, 2019.

[14] D. Yu, W. Hongxiang, and J. Yuefeng, "Experimental demonstration of all-optical aggregation and de-aggregation for a QPSK signal in an elastic optical network," *Opt. Exp.*, vol. 30, no. 5, pp. 6456–6468, 2022.

[15] L. Hong, W. Hongxiang, and J. Yuefeng, "Simultaneous all-optical channel aggregation and de-aggregation for 8QAM signal in elastic optical networking," *IEEE Photon. J.*, vol. 11, no. 1, pp. 1–8, Feb. 2019.

[16] F. Parmigiani, K. R. H. Bottrill, R. Slavk, D. J. Richardson, and P. Petropoulos, "Multi-channel phase regenerator based on polarization-assisted phase-sensitive amplification," *IEEE Photon. Technol. Lett.*, vol. 28, no. 8, pp. 845–848, Apr. 2016.

[17] L. Lu, P. G. Patki, T. I. Lakoba, and M. Vasilyev, "Simultaneous nonlinear-optical processing of multiple WDM channels," *Photon. Switching Comput.*, vol. 28, no. 8, pp. 1–2, 2018.

[18] P. Guan et al., "Scalable WDM phase regeneration in a single phase-sensitive amplifier through optical time lenses," *Nature Commun.*, vol. 9, no. 1, pp. 1–11, 2018.

[19] B. H. Kolner and M. Nazarathy, "Temporal imaging with a time lens," *Opt. Lett.*, vol. 14, no. 12, pp. 630–632, 1989.

[20] H. C. H. Mulvad et al., "Time-domain optical Fourier transformation for OTDM-DWDM and DWDM-OTDM conversion," in *Proc. Int. Conf. Inf. Photon. Opt. Commun.*, 2011, pp. 1–3.

[21] J. Azana, N. K. Berger, B. Levit, and B. Fischer, "Spectral Fraunhofer regime: Time-to-frequency conversion by the action of a single time lens on an optical pulse," *Appl. Opt.*, vol. 43, no. 2, pp. 483–490, 2004.

[22] N. K. Kjøller, K. M. Røge, P. Guan, H. C. H. Mulvad, M. Galili, and L. K. Oxenløwe, "A novel phase-locking-free phase sensitive amplifier-based regenerator," *J. Lightw. Technol.*, vol. 34, no. 2, pp. 643–652, 2016.

[23] K. R. H. Bottrill, G. Hesketh, F. Parmigiani, D. J. Richardson, and P. Petropoulos, "Optimisation of amplitude limiters for phase preservation based on the exact solution to degenerate four-wave mixing," *Opt. Exp.*, vol. 24, no. 3, pp. 2774–2787, 2016.

[24] M. Song et al., "Flat-top supercontinuum generation via Gaussian pulse shaping," *Opt. Exp.*, vol. 29, no. 8, pp. 12001–12009, 2021.

[25] R. J. Essiambre, G. Kramer, P. J. Winzer, G. J. Foschini, and B. Goebel, "Capacity limits of optical fiber networks," *J. Lightw. Technol.*, vol. 28, no. 4, pp. 662–701, Feb. 2010.

[26] Y. Matsumoto, K. Mishina, D. Hisano, and A. Maruta, "All-optical PAM4 to 16QAM modulation format conversion using nonlinear optical loop mirror and 1:2 coupler," *IEICE Trans. Commun.*, vol. E103.B, no. 11, pp. 1272–1281, 2020.

[27] G. Huang, Y. Miyoshi, A. Maruta, and K. Kitayama, "All-optical technique for modulation format conversion from NRZ-OOK to RZ-16QAM employing nonlinear optical loop mirror with 1:2 coupler," *Opt. Exp.*, vol. 20, no. 24, pp. 27311–27321, 2012.